

An energy-based summation-by-parts finite difference method for the wave equation in second order form

Siyang Wang* Daniel Appelö† Gunilla Kreiss‡

May 6, 2022

Abstract

We develop an energy-based finite difference method for the wave equation in second order form. The spatial discretization satisfies a summation-by-parts (SBP) property. With boundary conditions and material interface conditions imposed weakly by the simultaneous-approximation-term (SAT) method, we derive energy estimates for the semi-discretization. In addition, error estimates are derived by the normal mode analysis. The energy-based discretization does not use any mesh-dependent parameter, even in the presence of Dirichlet boundary conditions and material interfaces. Furthermore, similar to upwind discontinuous Galerkin methods, numerical dissipation can be added to the discretization through the boundary conditions. We present numerical experiments that verify convergence and robustness of the proposed method.

Keywords: Finite difference methods; Summation by parts; Wave equation; Energy based; Normal mode analysis

1 Introduction

Many wave phenomena are governed by second order hyperbolic partial differential equations (PDEs), such as the wave equation, the elastic wave equation and Einstein's equations of general relativity. Also, equations that are formulated in first order form, such as Maxwell's equations, may often be reformulated in second order form [12]. When a second order formulation is available it is typically formulated using fewer variables and fewer derivative operators, which can be exploited in the design of faster numerical methods. Many physical models are derived using Euler-Lagrange formalism starting from an energy, and it is natural to look for numerical methods that track the dynamics of this energy. We have considered such energy-based numerical methods in the context of discontinuous Galerkin discretizations, [3, 4, 6]. Here we generalize those ideas to high order finite difference methods.

The classical dispersion error analysis by Kreiss and Olinger, [14], predicts that high order methods are more efficient than low order methods when used for the simulation of wave propagation problems with smooth coefficients. High order finite difference methods are computationally efficient for solving hyperbolic PDEs and such methods are also easy to implement if the simulation domains are not too complex.

*Department of Mathematics and Mathematical Statistics, Umeå University, Umeå, Sweden. Email: siyang.wang@umu.se

†Department of Computational Mathematics, Science & Engineering and Department of Mathematics, Michigan State University, East Lansing, USA. Email: appeloda@msu.edu. This work was supported by NSF Grant DMS-1913076. Any opinions, findings, and conclusions or recommendations expressed in this material are those of the authors and do not necessarily reflect the views of the National Science Foundation.

‡Department of Information Technology, Uppsala University, Uppsala, Sweden. Email: gunilla.kreiss@it.uu.se

In the distant past it was difficult to construct stable and high order accurate finite difference methods, but this challenge has now largely been overcome through the use of derivative approximations with the summation-by-parts (SBP) property [11], and boundary and interface conditions enforced through the use of ghost points [20, 21], or by the simultaneous-approximation-term (SAT) method [7].

Summation by parts operators for the second derivative $\frac{d^2}{dx^2}$ and their extension to variable coefficients can be found in [15, 18]. When these SBP operators are used together with the SAT method to impose boundary or interface conditions for the wave equation in a second order in time and space form, the resulting discretization bears similarity with the symmetric interior penalty discontinuous Galerkin method (SIPDG) [10]. As for SIPDG, coercivity requires that such SBP-SAT methods use a mesh-dependent penalty term. This penalty parameter, which depends on the material properties and the SBP operator, must be large enough for the method to be stable [1, 5, 16, 17]. Precise bounds on this penalty parameter may not be easy to determine a priori [8, 24], especially in the presence of grid interface conditions [16], curvilinear grids [23] and nonconforming grid interfaces [2, 24, 27].

In this paper, we present an energy-based discretization in the SBP-SAT framework. For problems with only Neumann boundary conditions, the proposed method is the same as the traditional SBP-SAT discretization in [18], but is different for problems with Dirichlet boundary conditions or grid interfaces, because our method does not use any mesh-dependent parameter. The method discretizes the wave equation in the velocity-displacement form, i.e. as a system with first order derivatives in time and second order derivatives in space. The resulting system of ordinary differential equations can then be evolved by a Runge-Kutta time integrator or a Taylor series method. As mentioned above, the method is inspired by our energy-based discontinuous Galerkin (DG) method [3, 4, 6]. We show that, just as the energy-based DG method, numerical dissipation can naturally be included in the method and is important for optimal accuracy. We also present a general framework for deriving error estimates by normal mode analysis and perform the detailed analysis for a fourth order discretization for the Dirichlet problem. We will use the same approach as in [25] to prove fourth order convergence rate for the dissipative discretization and third order convergence rate for the energy-conserving discretization, which agree well with our numerical verification.

The outline of the paper is as follows. We introduce the SBP concepts in Section 2. In Section 3, we construct our new SBP-SAT discretization for problems with boundaries and grid interfaces. Stability analysis and a priori error estimates by normal mode analysis are then derived. In Section 4, we present an efficient implementation of the method for higher dimensional problems. Numerical experiments verifying optimal accuracy and robustness are presented in Section 5. We end with concluding remarks in Section 6.

2 Preliminaries

Let P and Q be twice continuously differentiable functions in $[0, 1]$. We define the standard inner product and norm in $L^2([0, 1])$ as

$$(P, Q) = \int_0^1 PQ dx, \quad \|P\|^2 = (P, P).$$

The integration-by-parts principle reads

$$\int_0^1 PQ_{xx} dx = - \int_0^1 P_x Q_x dx + PQ_x|_0^1. \quad (1)$$

This principle (and its generalization in higher dimensions) is a useful tool to connect the energy dynamics of a system, with an energy consisting of a kinetic and potential part, i.e.

$$E = \|U_t\|^2 + \|cU_x\|^2, \quad (2)$$

with eigenvalues

$$\lambda_j = 4 \sin^2 \left(\frac{\pi(j-1)}{2n} \right), \quad j = 1, 2, \dots, n.$$

We observe that all eigenvalues are distinct. Since $\lambda_1 = 0$, the rank of A is $n - 1$. For the fourth and sixth order SBP operators with constant coefficients, Assumption 2 is proved in [9], where the explicit formulas for the Moore-Penrose inverse of A are also derived.

2.2 Accuracy of SBP operators

Standard central finite difference stencils are used in the interior of the computational domain. To satisfy the SBP property, special non-centered difference stencils are used on a few grid points close to boundaries. In the interior where the central stencils are used, the truncation error is of even order, often denoted by $2p$ with $p = 1, 2, 3, \dots$. On a few grid points with the non-centered boundary stencils, the truncation error can at best be of order p when H is diagonal. We denote the accuracy of such SBP operators $(2p, p)$. Note that it is also common to refer to the accuracy of the operator and scheme as $2p^{\text{th}}$ order accurate. It is then important to be specific with the precise truncation error and convergence rate of the discretization.

Though the boundary truncation error is order p , the convergence rate of the underlying numerical scheme can be higher in certain cases. This is in part due to the fact that the number of grid points with the less accurate boundary stencils is independent of grid spacing. The precise order of convergence rate depends on the equation, the spatial discretization and the numerical boundary conditions, see further the detailed error analysis in [25, 26]. Below, in Section 3.2, we derive error estimates for the proposed scheme and we see that the choice of the SAT affects the convergence rate.

3 An energy-based SBP-SAT finite difference method

In this section, we derive the energy-based SBP-SAT discretization of the wave equation (3). First, we consider boundary conditions in Section 3.1. We show our method is equivalent to that in [17] for Neumann boundary conditions, but is different from the discretization in [17] for Dirichlet boundary conditions. We then derive error estimates in Section 3.2 and consider grid interface conditions in Section 3.3.

3.1 The boundary conditions

Our SBP-SAT discretization is based on the approximation of the unknown variable U and its time derivative U_t . Therefore, we rewrite equation (3) to a system with first order derivative in time

$$\begin{aligned} U_t &= V, \\ V_t &= (b(x)U_x)_x. \end{aligned} \tag{8}$$

The energy-based SBP-SAT finite difference approximation of (8) with the boundary condition (4) is

$$A^{(b)}(\mathbf{u}_t - \mathbf{v}) = b_1 \mathbf{d}_1 (\mathbf{e}_1^T \mathbf{v} - f_t) + \alpha \mathbf{d}_n (\mathbf{d}_n^T \mathbf{u} - g), \tag{9}$$

$$\mathbf{v}_t = D^{(b)} \mathbf{u} - b_n H^{-1} \mathbf{e}_n (\mathbf{d}_n^T \mathbf{u} - g) + \beta H^{-1} \mathbf{e}_1 (\mathbf{e}_1^T \mathbf{v} - f_t), \tag{10}$$

where \mathbf{u} and \mathbf{v} are grid functions that approximate U and V , respectively. On the right-hand side of (9), the first term imposes weakly the time derivative of the Dirichlet boundary condition $U_t(0, t) = f_t(t)$. This penalty term has contribution to a few grid points near the left boundary and the contribution is weighted by the stencil in \mathbf{d}_1 . The second term is a dissipative term

controlled by α and contributes to a few grid points near the right boundary. On the left-hand side, \mathbf{u}_t is approximately equal to \mathbf{v} . The symmetric positive semidefinite matrix $A^{(b)}$ is multiplied by $\mathbf{u}_t - \mathbf{v}$. In the traditional way of imposing the Dirichlet boundary condition in the SBP-SAT finite difference method, the corresponding penalty term is based on $U(0, t) = f(t)$ and involves a mesh-dependent penalty parameter [17]. This is not needed in our energy-based discretization.

In (10), the Neumann boundary condition is imposed weakly in the same way as in [18]. The last term on the right-hand side is a dissipation term that has contribution only on the first grid point and is controlled by the parameter β . The stability property of the semi-discretization is stated in the following theorem.

Theorem 1. *With homogeneous boundary conditions, the energy-based SBP-SAT discretization (9)-(10) with $\alpha \leq 0$ and $\beta \leq 0$ satisfies*

$$\frac{d}{dt}E_H = 2\alpha(\mathbf{d}_n^T \mathbf{u})^2 + 2\beta(\mathbf{e}_1^T \mathbf{v})^2 \leq 0.$$

The discrete energy E_H is defined as

$$E_H \equiv (\|u\|_{A^{(b)}}^2 + \|v\|_H^2),$$

and is the discrete analogue of the continuous energy (2).

Proof. Consider homogeneous boundary conditions with $f = g = 0$ in (4). By multiplying \mathbf{u}^T on both sides of (9), and $\mathbf{v}^T H$ on both sides of (10), we obtain

$$\mathbf{u}^T A^{(b)}(\mathbf{u}_t - \mathbf{v}) = b_1 \mathbf{u}^T \mathbf{d}_1 \mathbf{e}_1^T \mathbf{v} + \alpha \mathbf{u}^T \mathbf{d}_n \mathbf{d}_n^T \mathbf{u}, \quad (11)$$

$$\mathbf{v}^T H \mathbf{v}_t = \mathbf{v}^T H D^{(b)} \mathbf{u} - b_n \mathbf{v}^T \mathbf{e}_n \mathbf{d}_n^T \mathbf{u} + \beta \mathbf{v}^T \mathbf{e}_1 \mathbf{e}_1^T \mathbf{v}. \quad (12)$$

Adding (11) and (12), we have

$$\frac{d}{dt}E_H \equiv \frac{d}{dt}(\|u\|_{A^{(b)}}^2 + \|v\|_H^2) = 2\alpha(\mathbf{d}_n^T \mathbf{u})^2 + 2\beta(\mathbf{e}_1^T \mathbf{v})^2 \leq 0,$$

if $\alpha \leq 0$ and $\beta \leq 0$. □

If $\alpha < 0$ and $\beta < 0$, the discrete energy E_H is dissipated even though the continuous energy is conserved. With $\alpha = \beta = 0$, the discrete energy is constant in time.

In the first semi-discretized equation (9), the time derivative of the unknown variable \mathbf{u} is multiplied by $A^{(b)}$. The matrix $A^{(b)}$ is banded and symmetric positive semi-definite, with nullspace consisting of vectors of constants. Since both \mathbf{d}_1 and \mathbf{d}_n are consistent finite difference stencils for the first derivative, the right hand side will always be in the range of $A^{(b)}$. In other words, the solution exists but is only unique up to a constant. A unique solution can be obtained with an additional constraint. Here we require that the sum of all elements in $\mathbf{u}_t - \mathbf{v}$ are zero, consistent with the equation $U_t = V$. Numerically this constraint can be taken into account by the Lagrange multiplier technique. With the new variables

$$\tilde{A}^{(b)} = \begin{bmatrix} & & & 1 \\ & A^{(b)} & & \vdots \\ & & & 1 \\ 1 & \dots & 1 & 0 \end{bmatrix}, \quad \tilde{\mathbf{u}} = \begin{bmatrix} \mathbf{u} \\ \mu \end{bmatrix}, \quad \tilde{\mathbf{v}} = \begin{bmatrix} \mathbf{v} \\ \nu \end{bmatrix}, \quad \tilde{\mathbf{d}}_1 = \begin{bmatrix} \mathbf{d}_1 \\ 0 \end{bmatrix}, \quad \tilde{\mathbf{d}}_n = \begin{bmatrix} \mathbf{d}_n \\ 0 \end{bmatrix},$$

equation (9) is replaced by

$$\tilde{A}^{(b)}(\tilde{\mathbf{u}}_t - \tilde{\mathbf{v}}) = b_1 \tilde{\mathbf{d}}_1 (\mathbf{e}_1^T \mathbf{v} - f_t) + \alpha \tilde{\mathbf{d}}_n (\mathbf{d}_n^T \mathbf{u} - g), \quad (13)$$

which is nonsingular. The auxiliary variables μ and ν satisfy $\mu_t \approx \nu$.

Remark. At first glance it appears that the formulation (9) would have a higher computational complexity than comparable methods but, as we show in Section 4, for constant coefficient systems there is a fast direct algorithm that results in a linear (in the number of degrees of freedom) complexity. For variable coefficients we will illustrate by numerical examples that the preconditioned conjugate gradient method only requires a very small number of iterations per timestep to converge.

3.2 Error estimates

As discussed in Section 2.2, the $2p^{\text{th}}$ order accurate SBP operators with diagonal norms are only p^{th} order accurate on a few grid points near boundaries. In this section, we derive error estimates and analyze the effect of the p^{th} order truncation error on the overall convergence rate of the discretization. We note that the energy-based discretization for the Neumann problem is the same as the traditional SBP-SAT method [18] and for this problem the error estimates derived in [25] already applies. Below we consider the problem with Dirichlet boundary conditions by first outlining the general approach for error analysis and then specializing to the case when $p = 2$. As will be seen, dissipation at the Dirichlet boundary conditions improves convergence rate. We note that the influence of dissipation for a discretization of the wave equation is also considered in [22].

Consider the following half line problem

$$\begin{aligned} U_t &= V, \\ V_t &= U_{xx}, \end{aligned}$$

in the domain $x \in [0, \infty)$ with the Dirichlet boundary condition $U(0, t) = f(t)$ and $t \in [0, t_f]$ for some final time t_f . The corresponding energy-based discretization is

$$\begin{aligned} A(\mathbf{u}_t - \mathbf{v}) &= \mathbf{d}_1(\mathbf{e}_1^T \mathbf{v} - f_t), \\ \mathbf{v}_t &= D\mathbf{u} + \beta H^{-1} \mathbf{e}_1(\mathbf{e}_1^T \mathbf{v} - f_t). \end{aligned}$$

When $\beta \leq 0$, the discretization satisfies an energy estimate as in Theorem 1. We will see below that the energy-dissipative discretization with $\beta < 0$ gives a higher convergence rate than the energy-conserving discretization with $\beta = 0$.

Let $\boldsymbol{\xi} = [\xi_1, \xi_2, \dots]^T$ and $\boldsymbol{\zeta} = [\zeta_1, \zeta_2, \dots]^T$ be the pointwise error vector with $\xi_j = u_j(t) - U(x_j, t)$ and $\zeta_j = v_j(t) - V(x_j, t)$. We then have the error equations

$$\begin{aligned} A(\boldsymbol{\xi}_t - \boldsymbol{\zeta}) &= \mathbf{d}_1 \mathbf{e}_1^T \boldsymbol{\zeta}, \\ \boldsymbol{\zeta}_t &= D\boldsymbol{\xi} + \beta H^{-1} \mathbf{e}_1 \mathbf{e}_1^T \boldsymbol{\zeta} + \mathbf{T}, \end{aligned}$$

where \mathbf{T} is the truncation error vector. We partition the truncation error into two parts, the boundary truncation error \mathbf{T}^B and the interior truncation error \mathbf{T}^I such that $\mathbf{T} = \mathbf{T}^B + \mathbf{T}^I$. The only nonzero elements of \mathbf{T}^B are the first r elements corresponding to the boundary stencil of D and are of order $\mathcal{O}(h^p)$, where r depends on p but not h . In \mathbf{T}^I , the first r elements are zero and the rest are of order $\mathcal{O}(h^{2p})$ corresponding to the interior stencil of D .

We partition the error as $\boldsymbol{\xi} = \boldsymbol{\xi}^I + \boldsymbol{\xi}^B$ and $\boldsymbol{\zeta} = \boldsymbol{\zeta}^I + \boldsymbol{\zeta}^B$. The first terms $\boldsymbol{\xi}^I, \boldsymbol{\zeta}^I \sim \mathcal{O}(h^{2p})$ are caused by the interior truncation error \mathbf{T}^I and can be estimated by the energy technique for SBP methods. It is often the second part, $\boldsymbol{\xi}^B, \boldsymbol{\zeta}^B$ caused by the boundary truncation error \mathbf{T}^B , that determine the overall convergence rate of the scheme. We note that $\boldsymbol{\xi}^B, \boldsymbol{\zeta}^B$ satisfy the error equations

$$A((\boldsymbol{\xi}^B)_t - \boldsymbol{\zeta}^B) = \mathbf{d}_1 \mathbf{e}_1^T \boldsymbol{\zeta}^B, \tag{14}$$

$$(\boldsymbol{\zeta}^B)_t = D\boldsymbol{\xi}^B + \beta H^{-1} \mathbf{e}_1 \mathbf{e}_1^T \boldsymbol{\zeta}^B + \mathbf{T}^B. \tag{15}$$

For convenience, we define the h -independent quantities

$$\bar{A} = hA, \quad \bar{H} = \frac{1}{h}H, \quad \bar{\mathbf{d}}_1 = h\mathbf{d}_1,$$

and the new variables

$$\boldsymbol{\delta}_t = \boldsymbol{\zeta}^{\mathbf{B}} \text{ and } \boldsymbol{\varepsilon} = \boldsymbol{\xi}^{\mathbf{B}} - \boldsymbol{\delta}. \quad (16)$$

Next, we take the Laplace transform of the error equations (14)-(15) in time, and obtain the difference equations

$$\bar{A}\widehat{\boldsymbol{\varepsilon}} - \bar{\mathbf{d}}_1\mathbf{e}_1^T\widehat{\boldsymbol{\delta}} = \mathbf{0}, \quad (17)$$

$$\mathbf{e}_1\bar{\mathbf{d}}_1^T\widehat{\boldsymbol{\varepsilon}} + (\tilde{s}^2\bar{H} + \bar{A} + \mathbf{e}_1\bar{\mathbf{d}}_1^T + \bar{\mathbf{d}}_1\mathbf{e}_1^T - \beta\tilde{s}\mathbf{e}_1\mathbf{e}_1^T)\widehat{\boldsymbol{\delta}} = h^2\tilde{H}\mathbf{T}^{\mathbf{B}}, \quad (18)$$

where $\widehat{\boldsymbol{\varepsilon}}$ and $\widehat{\boldsymbol{\delta}}$ are the Laplace-transform of $\boldsymbol{\varepsilon}$ and $\boldsymbol{\delta}$, respectively. We also use the notation $\tilde{s} = sh$, where s is the dual of time.

In Laplace space, we solve the difference equations (17)-(18) and use (16) to derive an error estimate for $\widehat{\boldsymbol{\xi}}^{\mathbf{B}}$. The corresponding error estimate for $\boldsymbol{\xi}^{\mathbf{B}}$ in physical space can then be obtained by Parseval's relation. The precise estimate depends on the operators in (17)-(18). Below we consider the SBP operator with accuracy $(2p, p) = (4, 2)$ constructed in [18].

Theorem 2. *With the SBP operator of accuracy order (4,2) from [18], the method (17)-(18) has convergence rate four with a dissipative discretization $\beta < 0$. For the energy-conserving discretization with $\beta = 0$, the convergence rate is three.*

Proof. In this case, $\mathbf{T}^{\mathbf{B}}$ in (18) is to the leading order

$$\mathbf{T}^{\mathbf{B}} = h^2 U_{xxxx}(0, t) \left[\frac{11}{12}, -\frac{1}{12}, \frac{5}{516}, \frac{11}{588}, 0, 0, \dots \right]^T.$$

The accuracy analysis follows the same procedure when other SBP operators are used.

In (17), the matrix \bar{A} has boundary stencils in the first four rows and repeated interior stencil from row five. The matrix $\bar{\mathbf{d}}_1\mathbf{e}_1^T$ has only nonzero elements in the first four rows. Therefore, from row five the difference equation takes the form

$$\frac{1}{12}\widehat{\varepsilon}_{j-2} - \frac{4}{3}\widehat{\varepsilon}_{j-1} + \frac{5}{2}\widehat{\varepsilon}_j - \frac{4}{3}\widehat{\varepsilon}_{j+1} + \frac{1}{12}\widehat{\varepsilon}_{j+2} = 0, \quad j = 5, 6, \dots$$

The corresponding characteristic equation

$$\frac{1}{12}\lambda^4 - \frac{4}{3}\lambda^3 + \frac{5}{2}\lambda^2 - \frac{4}{3}\lambda + \frac{1}{12} = 0$$

has four solutions $7 - 4\sqrt{3} \approx 0.0718$, $7 + 4\sqrt{3} \approx 13.9282$, and a double root 1. The only admissible solution satisfying $|\lambda| < 1$ is $\lambda = 7 - 4\sqrt{3}$. As a consequence, the elements of the vector $\widehat{\boldsymbol{\varepsilon}}$ can be written as

$$\widehat{\boldsymbol{\varepsilon}} = [\widehat{\varepsilon}_1, \widehat{\varepsilon}_2, \widehat{\varepsilon}_3, \sigma, \sigma\lambda, \sigma\lambda^2, \sigma\lambda^3, \dots]^T,$$

with four unknowns $\widehat{\varepsilon}_1$, $\widehat{\varepsilon}_2$, $\widehat{\varepsilon}_3$ and σ . These four unknowns, together with the unknowns in $\widehat{\boldsymbol{\delta}}$, are involved in the first four equations of (17). To solve for them, we also need to consider (18).

The difference equation from row five of (18) takes the form

$$\frac{1}{12}\kappa^4 - \frac{4}{3}\kappa^3 + \left(\frac{5}{2} + \tilde{s}^2\right)\kappa^2 - \frac{4}{3}\kappa + \frac{1}{12} = 0,$$

and has two admissible roots

$$\kappa_1 = 7 - 4\sqrt{3} + \mathcal{O}(\tilde{s}^2), \quad \kappa_2 = 1 - \mathcal{O}(\tilde{s}).$$

We note that the second admissible root κ_2 is a slowly decaying component at $\tilde{s} \rightarrow 0^+$. The vector $\widehat{\boldsymbol{\delta}}$ can then be written as

$$\widehat{\boldsymbol{\delta}} = [\widehat{\delta}_1, \widehat{\delta}_2, \sigma_1 + \sigma_2, \sigma_1\kappa_1 + \sigma_2\kappa_2, \sigma_1\kappa_1^2 + \sigma_2\kappa_2^2, \sigma_1\kappa_1^3 + \sigma_2\kappa_2^3, \dots]^T,$$

with four unknowns $\widehat{\delta}_1$, $\widehat{\delta}_2$, σ_1 and σ_2 .

The first four equations of (17) and the first four equations of (18) lead to the eight-by-eight boundary system

$$C(\tilde{s}, \beta)\mathbf{z} = T_{uv}, \quad (19)$$

where the unknown vector \mathbf{z} and the right-hand side vector T_{uv} are

$$\begin{aligned} \mathbf{z} &= [\widehat{\varepsilon}_1, \widehat{\varepsilon}_2, \widehat{\varepsilon}_3, \sigma, \widehat{\delta}_1, \widehat{\delta}_2, \sigma_1, \sigma_2]^T, \\ T_{uv} &= \left[0, 0, 0, 0, \frac{187}{576}, -\frac{59}{576}, \frac{5}{576}, \frac{11}{576} \right]^T h^4 \widehat{U}_{xxxx}(0, t). \end{aligned} \quad (20)$$

From (16), we have

$$\begin{aligned} \widehat{\boldsymbol{\xi}}^B &= \widehat{\boldsymbol{\varepsilon}} + \widehat{\boldsymbol{\delta}} \\ &= [\widehat{\varepsilon}_1 + \widehat{\delta}_1, \widehat{\varepsilon}_2 + \widehat{\delta}_2, \widehat{\varepsilon}_3 + \sigma_1 + \sigma_2, \sigma + \sigma_1\kappa_1 + \sigma_2\kappa_2, \sigma\lambda + \sigma_1\kappa_1^2 + \sigma_2\kappa_2^2, \dots]^T, \end{aligned} \quad (21)$$

which depends on all the eight unknowns in the vector \mathbf{z} .

For the L_2 convergence rate of the solution \mathbf{u} , we shall analyze the components of \mathbf{z} in the vicinity of $\tilde{s} \rightarrow 0^+$ corresponding to the asymptotic region when $h \rightarrow 0$. When the scheme is stable with $\beta \leq 0$, the matrix $C(\tilde{s}, \beta)$ is non-singular for all $Re(\tilde{s}) > 0$ [11]. However, the inverse of $C(\tilde{s}, \beta)$, and consequently \mathbf{z} , may depend on $\tilde{s} = sh$. The dependence of \mathbf{z} on h is vital to the precise convergence rate of the proposed scheme. In the following, we analyze \mathbf{z} and $\widehat{\boldsymbol{\xi}}^B$ in the vicinity of $\tilde{s} \rightarrow 0^+$.

We start by considering the boundary system (19) with $\tilde{s} = 0$. Here, the matrix $C(0) := C(0, \beta)$ is independent of β and is singular with one eigenvalue equal to zero, i.e. the so-called determinant condition is not satisfied [11]. Since the matrix $C(\tilde{s}, \beta)$ cannot be inverted at $\tilde{s} = 0$, we take a similar approach as in [19, 25] and consider $Re(\tilde{s}) = \eta h$ for a small constant $\eta > 0$ independent of h .

The Taylor series of $C(\tilde{s}, \beta)$ at $\tilde{s} = 0$ can be written as

$$C(\tilde{s}, \beta) = C(0) + \tilde{s}C'(0, \beta) + \frac{\tilde{s}^2}{2}C''(0, \beta) + \mathcal{O}(\tilde{s}^3), \quad (22)$$

where $C'(0, \beta)$ and $C''(0, \beta)$ are the first and second derivative of $C(\tilde{s}, \beta)$ with respect to \tilde{s} at $\tilde{s} = 0$, respectively. We perform a singular value decomposition of the singular matrix $C(0) = M\Sigma N^*$ with two unitary matrices M and N . Substituting into the Taylor series, we obtain the boundary system to the leading order

$$(\Sigma + \tilde{s}C_\beta)\bar{\mathbf{z}} = M^*T_{uv}, \quad (23)$$

where $\bar{\mathbf{z}} = N^*\mathbf{z}$ and $C_\beta = M^*C'(0, \beta)N$. The solution can be written as

$$\bar{\mathbf{z}} = (\Sigma + \tilde{s}C_\beta)^{-1}M^*T_{uv},$$

and consequently we have

$$\mathbf{z} = N(\Sigma + \tilde{s}C_\beta)^{-1}M^*T_{uv}.$$

We note that Σ is a diagonal matrix where the first seven diagonal components are nonzero and the last diagonal component equals to zero. The last diagonal element of C_β , denoted by $(C_\beta)_{88}$,

is crucial. We find that $(C_\beta)_{88}$ is zero when $\beta = 0$ and nonzero when $\beta < 0$. We analyze these two cases separately.

When $\beta < 0$, we have $(C_\beta)_{88} \neq 0$. In this case, we have

$$(\Sigma + \tilde{s}C_\beta)_{ij} = \begin{cases} \mathcal{O}(1), & 1 \leq i = j \leq 7 \\ \mathcal{O}(\tilde{s}), & i = j = 8, \\ \mathcal{O}(\tilde{s}) \text{ or } 0, & i \neq j. \end{cases}$$

The linear system (23) can be solved by Gaussian elimination. The resulting upper triangular matrix has diagonal elements $\mathcal{O}(1)$, except the last diagonal element $\mathcal{O}(\tilde{s})$. Using that all elements of M^*T_{uv} are $\mathcal{O}(h^4)$, the backward substitution procedure gives the solution $\bar{\mathbf{z}}$ in the form such that its first seven elements are $\mathcal{O}(h^4)$ and the last element is $\mathcal{O}(\tilde{s}^{-1}h^4) \sim \mathcal{O}(h^3)$.

The dominating error component $\mathcal{O}(h^3)$ in $\bar{\mathbf{z}}$ is a potential source of accuracy reduction. To analyze its effect to the convergence rate, we only consider this dominating component in $\bar{\mathbf{z}}$, that is $[0, 0, 0, 0, 0, 0, 0, 1]^T Kh^3$ for some constant K . By the relation $\mathbf{z} = N\bar{\mathbf{z}}$, the corresponding part of \mathbf{z} can be computed as $\mathbf{z} = N[0, 0, 0, 0, 0, 0, 0, 1]^T Kh^3$. The elements of \mathbf{z} satisfy the following relations,

$$\widehat{\varepsilon}_1 + \widehat{\delta}_1 = \widehat{\varepsilon}_2 + \widehat{\delta}_2 = \widehat{\varepsilon}_3 + \sigma_1 = 0, \quad \sigma + \sigma_1\kappa_1 = 0, \quad \sigma_2 = 0. \quad (24)$$

The last relation $\sigma_2 = 0$ is important because in the error vector (21), the variable σ_2 is multiplied with the slowly decaying component κ_2 , which is now eliminated. By using the first relation in (24) and the relation $\lambda = \kappa_1 + \mathcal{O}(\tilde{s}^2)$, the error vector (21) becomes

$$\widehat{\boldsymbol{\xi}}^{\mathbf{B}} = h^3[0, 0, 0, 0, \mathcal{O}(\tilde{s}^2), \mathcal{O}(\tilde{s}^4), \dots]^T.$$

Therefore, the dominating error component $\mathcal{O}(h^3)$ in $\bar{\mathbf{z}}$ does not lead to a convergence rate reduction. As a consequence, the error $\widehat{\boldsymbol{\xi}}^{\mathbf{B}}$ is determined by the first seven elements of $\bar{\mathbf{z}} \sim \mathcal{O}(h^4)$. It is then straightforward to compute

$$\|\widehat{\boldsymbol{\xi}}^{\mathbf{B}}\|_h \leq \tilde{K}h^{4.5}|\widehat{U}_{xxxx}(0, t)|$$

for some constant \tilde{K} . By using Parseval's relation, we have

$$\int_0^{t_f} \|\widehat{\boldsymbol{\xi}}^{\mathbf{B}}\|_h dt \leq Kh^{4.5}e^{2\eta t_f} \int_0^{t_f} |U_{xxxx}(0, t)| dt$$

for some constant K . In the above, we have used the argument ‘‘future cannot affect past’’ [11, pp. 294]. Finally, the overall error $\boldsymbol{\xi}$ is in fact determined by the interior scheme. We conclude that the scheme has a fourth order convergence rate when $\beta < 0$.

Now, we consider the case $\beta = 0$. Since $(U_c^*C'(0, \beta)V_c)_{88} = 0$, it is necessary to include the quadratic term of the Taylor series (22) in the boundary system analysis. A direct calculation gives $(U_c^*C''(0, \beta)V_c)_{88} \neq 0$. The solution $\bar{\mathbf{z}}$ to the boundary system is then in the form such that its first seven components are $\mathcal{O}(h^3)$ and the last component is $\mathcal{O}(h^2)$. The dominating error component $\mathcal{O}(h^2)$ does not lead to a convergence rate reduction for the same reason as the case with $\beta < 0$. However, the other seven components $\mathcal{O}(h^3)$ lead to $\|\widehat{\boldsymbol{\xi}}^{\mathbf{B}}\|_h \leq K_3h^3|\widehat{U}_{xxxx}(0, t)|$ for some constant K_3 . Note that in this case, the slowly decaying component κ_2 does not vanish in $\widehat{\boldsymbol{\xi}}^{\mathbf{B}}$. Therefore, the convergence rate is three when $\beta = 0$. This concludes the proof. \square

3.3 Interface conditions

In heterogeneous materials, a multi-block finite difference discretization can be advantageous. Different grid spacings can be used in different blocks to adapt to the velocity structure of the

material. If the material property is discontinuous, the material interfaces can be aligned with block boundaries so that high order accurate discretization can be constructed in each block.

As a model problem, we again consider the wave equation (8) in the domain $[-1,1]$. The parameter $b(x)$ is smooth in $(-1,0)$ and $(0,1)$, but discontinuous at $x = 0$. In the stability analysis, we omit terms corresponding to the boundaries $x = 0, 1$ and focus on the interface contribution. The energy (2) is conserved in time if we impose the interface conditions

$$\lim_{\epsilon \rightarrow 0^+} U(-\epsilon, t) = \lim_{\epsilon \rightarrow 0^+} U(\epsilon, t), \quad (25)$$

$$\lim_{\epsilon \rightarrow 0^+} b(-\epsilon)U_x(-\epsilon, t) = \lim_{\epsilon \rightarrow 0^+} b(\epsilon)U_x(\epsilon, t). \quad (26)$$

In this case, at $x = 0$ the solution is continuous but its derivative is discontinuous.

We proceed by deriving an energy-based SBP-SAT discretization. To distinguish notations in the two subdomains, we use a tilde symbol on top of the variables and operators in $[0, 1]$. The semi-discretization reads

$$A^{(b)}(\mathbf{u}_t - \mathbf{v}) = -\tau b_n \mathbf{d}_n (\mathbf{e}_n^T \mathbf{v} - \tilde{\mathbf{e}}_1^T \tilde{\mathbf{v}}), \quad (27)$$

$$\mathbf{v}_t = D^{(c)} \mathbf{u} - (1 - \tau) H^{-1} \mathbf{e}_n (b_n \mathbf{d}_n^T \mathbf{u} - \tilde{b}_1 \tilde{\mathbf{d}}_1^T \tilde{\mathbf{u}}) + \gamma H^{-1} \mathbf{e}_n (\mathbf{e}_n^T \mathbf{v} - \tilde{\mathbf{e}}_1^T \tilde{\mathbf{v}}), \quad (28)$$

in the subdomain $[-1, 0]$, and

$$\tilde{A}^{(b)}(\tilde{\mathbf{u}}_t - \tilde{\mathbf{v}}) = (1 - \tau) \tilde{b}_1 \tilde{\mathbf{d}}_1 (\tilde{\mathbf{e}}_1^T \tilde{\mathbf{v}} - \mathbf{e}_n^T \mathbf{v}), \quad (29)$$

$$\tilde{\mathbf{v}}_t = \tilde{D}^{(b)} \tilde{\mathbf{u}} + \tau \tilde{H}^{-1} \tilde{\mathbf{e}}_1 (\tilde{b}_1 \tilde{\mathbf{d}}_1^T \tilde{\mathbf{u}} - b_n \mathbf{d}_n^T \mathbf{u}) + \gamma \tilde{H}^{-1} \tilde{\mathbf{e}}_1 (\tilde{\mathbf{e}}_1^T \tilde{\mathbf{v}} - \mathbf{e}_n^T \mathbf{v}). \quad (30)$$

in the subdomain $[0, 1]$. Similar to the Dirichlet boundary condition, we impose continuity of the time derivative of the solution, instead of continuity of the solution itself. Unlike in [23], no mesh-dependent parameter is needed to impose interface conditions by the SAT method. The stability property is summarized in the following theorem.

Theorem 3. *The semi-discretization (27)-(30) satisfies*

$$\frac{d}{dt} E_H = 2\gamma (\mathbf{e}_n^T \mathbf{v} - \tilde{\mathbf{e}}_1^T \tilde{\mathbf{v}})^2 \leq 0,$$

where the discrete energy is defined as $E_H \equiv \|\mathbf{u}\|_{A^{(b)}}^2 + \|\mathbf{v}\|_H^2 + \|\tilde{\mathbf{u}}\|_{\tilde{A}^{(b)}}^2 + \|\tilde{\mathbf{v}}\|_{\tilde{H}}^2$ for any τ and $\gamma \leq 0$.

Proof. We multiply (27) by \mathbf{u}^T , (28) by $\mathbf{v}^T H^{-1}$, (29) by $\tilde{\mathbf{u}}^T$, (30) by $\tilde{\mathbf{v}}^T \tilde{H}^{-1}$. After adding all the four equations, we obtain

$$\frac{d}{dt} E_H = 2\gamma (\mathbf{e}_n^T \mathbf{v} - \tilde{\mathbf{e}}_1^T \tilde{\mathbf{v}})^2,$$

where the discrete energy is $E_H = \|\mathbf{u}\|_{A^{(b)}}^2 + \|\mathbf{v}\|_H^2 + \|\tilde{\mathbf{u}}\|_{\tilde{A}^{(b)}}^2 + \|\tilde{\mathbf{v}}\|_{\tilde{H}}^2$. We then have $\frac{d}{dt} E_H \leq 0$ when $\gamma \leq 0$. In particular, if $\gamma = 0$, then the discrete energy is conserved in time. \square

We note that the linear system involving $A^{(b)}$ and $\tilde{A}^{(b)}$ can be solved separately in each domain, thus resulting a linear computational complexity with respect to the number of degrees of freedom.

4 Discretization in higher space dimensions

The one-dimensional discretization technique can be generalized to higher dimensional problems by tensor products. As an example, we consider the wave equation in two space dimensions (2D)

$$\begin{aligned} U_t &= V, \\ V_t &= (a(x, y)U_x)_x + (b(x, y)U_y)_y + F, \end{aligned} \quad (31)$$

in the domain $\Omega = [0, 1]^2$ with Dirichlet boundary conditions

$$U(x, y, t) = f(x, y, t) \text{ on } \partial\Omega,$$

and a forcing function F . We discretize Ω by a Cartesian grid with n_x points in x and n_y points in y . The semi-discretization can be written as

$$\begin{aligned} \mathbf{A}(\mathbf{u}_t - \mathbf{v}) &= d_W H_y (e_W^T \mathbf{v} - \mathbf{f}_{tW}) - d_E H_y (e_E^T \mathbf{v} - \mathbf{f}_{tE}) \\ &\quad + d_S H_x (e_S^T \mathbf{v} - \mathbf{f}_{tS}) - d_N H_x (e_N^T \mathbf{v} - \mathbf{f}_{tN}), \end{aligned} \quad (32)$$

$$\begin{aligned} \mathbf{v}_t &= \mathbf{D}\mathbf{u} + \mathbf{F} + \theta \mathbf{H}^{-1} [e_W H_y (e_W^T \mathbf{v} - \mathbf{f}_{tW}) + e_E H_y (e_E^T \mathbf{v} - \mathbf{f}_{tE}) \\ &\quad + e_S H_x (e_S^T \mathbf{v} - \mathbf{f}_{tS}) + e_N H_x (e_N^T \mathbf{v} - \mathbf{f}_{tN})]. \end{aligned} \quad (33)$$

The operator \mathbf{D} in (33) approximates the second derivative with variable coefficients in 2D and is defined as

$$\mathbf{D} = \sum_{i=1}^{n_y} D^{a:,i} \otimes E_y^i + \sum_{j=1}^{n_x} E_x^j \otimes D^{b:,j},$$

where $D^{a:,i}$ approximates $\frac{\partial}{\partial x} (a(x, y_i) \frac{\partial}{\partial x})$ and the only nonzero element in the n_y by n_y matrix E_y^i is $E_y^i(i, i) = 1$. The operators corresponding to the term in the y -direction is defined similarly. The operator $\mathbf{H} = H_x \otimes H_y$ defines the 2D SBP norm and quadrature. In addition, we also have in (32) that

$$\mathbf{A} = \sum_{i=1}^{n_y} A^{a:,i} \otimes E_y^i H_y + \sum_{j=1}^{n_x} E_x^j H_x \otimes A^{b:,j},$$

where $A^{a:,i}$ is the symmetric semidefinite matrix associated with $D^{a:,i}$. The right-hand side of (32) are SAT imposing the Dirichlet boundary conditions. We define

$$\begin{aligned} d_W &= \sum_{i=1}^{n_y} d^{a1,i} \otimes E_y^i, \quad d_E = \sum_{i=1}^{n_y} d^{a_{nx},i} \otimes E_y^i, \\ d_S &= \sum_{j=1}^{n_x} E_x^j \otimes d^{b:,j}, \quad d_N = \sum_{j=1}^{n_x} E_x^j \otimes d^{b:,n_y}, \end{aligned}$$

where $d^{a1,i}$ approximates the first derivative $a(x_1, y_i) \frac{\partial}{\partial x}$ and is associated with $D^{a:,i}$. The n_y by 1 vector \mathbf{f}_{tW} is the time derivative of the Dirichlet boundary data evaluated on the grid of the left boundary $x = 0$. We use the following operators to select the numerical solutions on the boundary

$$e_W = e_{1x} \otimes I_y, \quad e_E = e_{nx} \otimes E_y^i, \quad e_S = I_x \otimes e_{1y}, \quad e_N = I_x \otimes e_{ny}.$$

Finally, the second term on the right-hand side of (33) corresponds to numerical dissipation and the parameter θ is determined by the energy analysis. The grid function \mathbf{F} is the forcing function F evaluated on the grid.

Theorem 4. *The semi-discretization (32)-(33) satisfies*

$$\frac{d}{dt} E_H \leq 0,$$

if $\theta \leq 0$, where the discrete energy is $E_H \equiv \mathbf{u}^T \mathbf{A} \mathbf{u} + \mathbf{v}^T \mathbf{H} \mathbf{v}$.

Proof. Consider homogeneous boundary and forcing data. Multiplying (32) by \mathbf{u}^T , we have

$$\mathbf{u}^T \mathbf{A} \mathbf{u}_t = \mathbf{u}^T \mathbf{A} \mathbf{v} + \mathbf{u}^T d_W H_y e_W^T \mathbf{v} - \mathbf{u}^T d_E H_y e_E^T \mathbf{v} + \mathbf{u}^T d_S H_x e_S^T \mathbf{v} - \mathbf{u}^T d_N H_x e_N^T \mathbf{v}. \quad (34)$$

Similarly, we multiply (33) by $\mathbf{v}^T \mathbf{H}$ and obtain

$$\begin{aligned} \mathbf{v}^T \mathbf{H} \mathbf{v}_t &= \mathbf{v}^T \mathbf{H} \mathbf{D} \mathbf{u} + \theta \mathbf{v}^T (e_W H_y e_W^T \mathbf{v} + e_E H_y e_E^T \mathbf{v} + e_S H_x e_S^T \mathbf{v} + e_N H_x e_N^T \mathbf{v}) \\ &= -\mathbf{v}^T \mathbf{A} \mathbf{u} - \mathbf{v}^T e_W H_y d_W^T \mathbf{u} + \mathbf{v}^T e_E H_y d_E^T \mathbf{u} - \mathbf{v}^T e_S H_x d_S^T \mathbf{u} + \mathbf{v}^T e_N H_x d_N^T \mathbf{u} \\ &\quad + \theta \mathbf{v}^T (e_W H_y e_W^T \mathbf{v} + e_E H_y e_E^T \mathbf{v} + e_S H_x e_S^T \mathbf{v} + e_N H_x e_N^T \mathbf{v}). \end{aligned} \quad (35)$$

We then add (34) and (35) to obtain

$$\begin{aligned} \frac{d}{dt} (\mathbf{u}^T \mathbf{A} \mathbf{u} + \mathbf{v}^T \mathbf{H} \mathbf{v}) &= 2\mathbf{u}^T \mathbf{A} \mathbf{u}_t + 2\mathbf{v}^T \mathbf{H} \mathbf{v}_t \\ &= 2\theta \mathbf{v}^T (e_W H_y e_W^T \mathbf{v} + e_E H_y e_E^T \mathbf{v} + e_S H_x e_S^T \mathbf{v} + e_N H_x e_N^T \mathbf{v}). \end{aligned} \quad (36)$$

Therefore, the discrete energy $E_H \equiv \mathbf{u}^T \mathbf{A} \mathbf{u} + \mathbf{v}^T \mathbf{H} \mathbf{v}$ decays in time if $\theta < 0$ and conserves in time if $\theta = 0$. \square

To advance in time the two dimensional semi-discretized equations (32)-(33), we need to isolate the \mathbf{u}_t term. In Section 4.1 we show that when the problem has constant coefficients this can be efficiently done through the diagonalization technique considered in [28]. In Section 4.2 we illustrate that the variable coefficient case can be handled by the use of iterative solvers.

4.1 Constant coefficient problems

Now consider the case $a(x, y) \equiv a$ and $b(x, y) \equiv b$, where a, b are positive constant. The semi-discretized equation is the same as (32)-(33) but the operators \mathbf{D} , \mathbf{A} and $d_{W,E,S,N}$ are in a simpler form

$$\begin{aligned} \mathbf{D} &= aD_x \otimes I_y + bI_x \otimes D_y, \quad \mathbf{A} = aA_x \otimes H_y + bH_x \otimes A_y, \\ d_W &= a\mathbf{d}_{1x} \otimes I_y, \quad d_E = a\mathbf{d}_{nx} \otimes I_y, \quad d_S = bI_x \otimes \mathbf{d}_{1y}, \quad d_N = bI_x \otimes \mathbf{d}_{ny}, \end{aligned}$$

where $D_x = H_x^{-1}(-A_x - e_{1x}\mathbf{d}_{1x}^T + e_{nx}\mathbf{d}_{nx}^T)$ approximates $\partial^2/\partial x^2$ and the operators with subscript y are defined analogously. We further define

$$\tilde{\mathbf{A}} = \mathbf{H}^{-\frac{1}{2}} \mathbf{A} \mathbf{H}^{-\frac{1}{2}} = \underbrace{(aH_x^{-\frac{1}{2}} A_x H_x^{-\frac{1}{2}})}_{\tilde{A}_x} \otimes I_y + I_x \otimes \underbrace{(bH_y^{-\frac{1}{2}} A_y H_y^{-\frac{1}{2}})}_{\tilde{A}_y}$$

and consider the eigendecomposition of \tilde{A}_x and \tilde{A}_y ,

$$\tilde{A}_x Q_x = Q_x \Lambda_x, \quad \tilde{A}_y Q_y = Q_y \Lambda_y.$$

Here, Λ_x is a diagonal matrix with the eigenvalues of \tilde{A}_x as the diagonal entries. Since \tilde{A}_x is real and symmetric, the eigenvectors can be chosen to be orthogonal $Q_x^T = Q_x^{-1}$. The operators Q_y and Λ_y are defined analogously. The operator $\tilde{\mathbf{A}}$ can be diagonalized as

$$\mathbf{Q}^T \tilde{\mathbf{A}} \mathbf{Q} = \Lambda,$$

where the orthogonal matrix $\mathbf{Q} = Q_x \otimes Q_y$ and the diagonal matrix $\Lambda = \Lambda_x \otimes I_y + I_x \otimes \Lambda_y$.

Next, we define $\tilde{\mathbf{u}}$ and $\tilde{\mathbf{v}}$ such that they satisfy

$$\mathbf{u} = \mathbf{H}^{-\frac{1}{2}} \mathbf{Q} \tilde{\mathbf{u}} \quad \text{and} \quad \mathbf{v} = \mathbf{H}^{-\frac{1}{2}} \mathbf{Q} \tilde{\mathbf{v}}, \quad (37)$$

respectively. Substituting the new variables into (32), we obtain

$$\begin{aligned} \mathbf{A}\mathbf{H}^{-\frac{1}{2}}\mathbf{Q}(\tilde{\mathbf{u}}_t - \tilde{\mathbf{v}}) &= d_W H_y \left(e_W^T \mathbf{H}^{-\frac{1}{2}} \mathbf{Q} \tilde{\mathbf{v}} - \mathbf{f}_{tW} \right) - d_E H_y \left(e_E^T \mathbf{H}^{-\frac{1}{2}} \mathbf{Q} \tilde{\mathbf{v}} - \mathbf{f}_{tE} \right) \\ &\quad + d_S H_x \left(e_S^T \mathbf{H}^{-\frac{1}{2}} \mathbf{Q} \tilde{\mathbf{v}} - \mathbf{f}_{tS} \right) - d_N H_x \left(e_N^T \mathbf{H}^{-\frac{1}{2}} \mathbf{Q} \tilde{\mathbf{v}} - \mathbf{f}_{tN} \right). \end{aligned}$$

After multiplying $(\mathbf{H}^{-\frac{1}{2}}\mathbf{Q})^T$ on both sides from the left, we have

$$\begin{aligned} \mathbf{\Lambda}(\tilde{\mathbf{u}}_t - \tilde{\mathbf{v}}) &= (\mathbf{H}^{-\frac{1}{2}}\mathbf{Q})^T \left[d_W H_y \left(e_W^T \mathbf{H}^{-\frac{1}{2}} \mathbf{Q} \tilde{\mathbf{v}} - \mathbf{f}_{tW} \right) - d_E H_y \left(e_E^T \mathbf{H}^{-\frac{1}{2}} \mathbf{Q} \tilde{\mathbf{v}} - \mathbf{f}_{tE} \right) \right. \\ &\quad \left. + d_S H_x \left(e_S^T \mathbf{H}^{-\frac{1}{2}} \mathbf{Q} \tilde{\mathbf{v}} - \mathbf{f}_{tS} \right) - d_N H_x \left(e_N^T \mathbf{H}^{-\frac{1}{2}} \mathbf{Q} \tilde{\mathbf{v}} - \mathbf{f}_{tN} \right) \right]. \end{aligned} \quad (38)$$

We note that the diagonal matrix $\mathbf{\Lambda}$ has one eigenvalue equal to zero. If we order the eigenvalues such that the first diagonal entry of $\mathbf{\Lambda}$ is zero, then we replace the first equation of (38) by $(\tilde{\mathbf{u}}_1)_t = \tilde{\mathbf{v}}_1$.

In the same way, we can substitute the new variables $\tilde{\mathbf{u}}$ and $\tilde{\mathbf{v}}$ into (33) and obtain

$$\begin{aligned} \mathbf{H}^{-\frac{1}{2}}\mathbf{Q}\tilde{\mathbf{v}}_t &= \mathbf{D}\mathbf{H}^{-\frac{1}{2}}\mathbf{Q}\tilde{\mathbf{u}} + \mathbf{F} \\ &\quad + \theta \mathbf{H}^{-1} [e_W H_y (e_W^T \mathbf{H}^{-\frac{1}{2}} \mathbf{Q} \tilde{\mathbf{v}} - \mathbf{f}_{tW}) + e_E H_y (e_E^T \mathbf{H}^{-\frac{1}{2}} \mathbf{Q} \tilde{\mathbf{v}} - \mathbf{f}_{tE}) \\ &\quad + e_S H_x (e_S^T \mathbf{H}^{-\frac{1}{2}} \mathbf{Q} \tilde{\mathbf{v}} - \mathbf{f}_{tS}) + e_N H_x (e_N^T \mathbf{H}^{-\frac{1}{2}} \mathbf{Q} \tilde{\mathbf{v}} - \mathbf{f}_{tN})]. \end{aligned}$$

By multiplying $\mathbf{Q}^T \mathbf{H}^{\frac{1}{2}}$ on both sides from the left, we have

$$\begin{aligned} \tilde{\mathbf{v}}_t &= \mathbf{Q}^T \mathbf{H}^{\frac{1}{2}} \mathbf{D} \mathbf{H}^{-\frac{1}{2}} \mathbf{Q} \tilde{\mathbf{u}} + \mathbf{Q}^T \mathbf{H}^{\frac{1}{2}} \mathbf{F} + \theta \mathbf{Q}^T \mathbf{H}^{-\frac{1}{2}} [e_W H_y (e_W^T \mathbf{H}^{-\frac{1}{2}} \mathbf{Q} \tilde{\mathbf{v}} - \mathbf{f}_{tW}) \\ &\quad + e_E H_y (e_E^T \mathbf{H}^{-\frac{1}{2}} \mathbf{Q} \tilde{\mathbf{v}} - \mathbf{f}_{tE}) + e_S H_x (e_S^T \mathbf{H}^{-\frac{1}{2}} \mathbf{Q} \tilde{\mathbf{v}} - \mathbf{f}_{tS}) + e_N H_x (e_N^T \mathbf{H}^{-\frac{1}{2}} \mathbf{Q} \tilde{\mathbf{v}} - \mathbf{f}_{tN})]. \end{aligned} \quad (39)$$

The transformed difference operator $\mathbf{Q}^T \mathbf{H}^{\frac{1}{2}} \mathbf{D} \mathbf{H}^{-\frac{1}{2}} \mathbf{Q}$ can be simplified by using the relation

$$\mathbf{D} = \mathbf{H}^{-1} (-\mathbf{A} - e_W H_y d_W^T + e_E H_y d_E^T - e_S H_x d_S^T + e_N H_x d_N^T)$$

to obtain

$$\begin{aligned} \mathbf{Q}^T \mathbf{H}^{\frac{1}{2}} \mathbf{D} \mathbf{H}^{-\frac{1}{2}} \mathbf{Q} &= \mathbf{Q}^T \mathbf{H}^{-\frac{1}{2}} (-\mathbf{A} - e_W H_y d_W^T + e_E H_y d_E^T - e_S H_x d_S^T + e_N H_x d_N^T) \mathbf{H}^{-\frac{1}{2}} \mathbf{Q} \\ &= -\mathbf{\Lambda} + \mathbf{Q}^T \mathbf{H}^{-\frac{1}{2}} (-e_W H_y d_W^T + e_E H_y d_E^T - e_S H_x d_S^T + e_N H_x d_N^T) \mathbf{H}^{-\frac{1}{2}} \mathbf{Q}. \end{aligned}$$

The operator \mathbf{A} , which is the volume part of \mathbf{D} , is diagonalized to $\mathbf{\Lambda}$. For the boundary parts, we do not need to use the $n_x n_y$ -by- $n_x n_y$ dense matrix \mathbf{Q} . As an example, for the term $\mathbf{Q}^T \mathbf{H}^{-\frac{1}{2}} e_W H_y d_W^T \mathbf{H}^{-\frac{1}{2}} \mathbf{Q}$, we have

$$\begin{aligned} &\mathbf{Q}^T \mathbf{H}^{-\frac{1}{2}} e_W H_y d_W^T \mathbf{H}^{-\frac{1}{2}} \mathbf{Q} \\ &= (Q_x^T \otimes Q_y^T) (H_x^{-\frac{1}{2}} \otimes H_y^{-\frac{1}{2}}) (e_{1x} \otimes I_y) (1 \otimes H_y) (a d_{1x}^T \otimes I_y) (H_x^{-\frac{1}{2}} \otimes H_y^{-\frac{1}{2}}) (Q_x \otimes Q_y) \\ &= (Q_x^T H_x^{-\frac{1}{2}} e_{1x} a d_{1x}^T H_x^{-\frac{1}{2}} Q_x) \otimes (Q_y^T H_y^{-\frac{1}{2}} H_y H_y^{-\frac{1}{2}} Q_y) \\ &= (Q_x^T H_x^{-\frac{1}{2}} e_{1x} a d_{1x}^T H_x^{-\frac{1}{2}} Q_x) \otimes I_y \end{aligned}$$

Furthermore, the rank of the n_x -by- n_x matrix $e_{1x} a d_{1x}^T$ is 1. Hence, multiplying the $n_x n_y$ -by- $n_x n_y$ matrix with the vector $\tilde{\mathbf{u}}$ can be done with computational complexity $\mathcal{O}(n_x n_y)$. This procedure can be used for the computation of the other boundary terms in (38) and (39). In the end, the solution to the original problem can be obtained by (37).

4.2 Variable coefficient problems

The above diagonalization procedure cannot be easily generalized to solve problems with variable coefficients (either originating from heterogeneous material properties or grid transformation). Instead we may simply solve $\mathbf{A}\mathbf{u}_t$ in each timestep by an iterative method. As \mathbf{A} is symmetric and since the right hand side will always be in the range of A the method of choice is the preconditioned conjugate gradient method. Below, in Section 5.2 we show that when an incomplete Cholesky preconditioner is used in together with the initial guess $\mathbf{u}_t \approx \mathbf{v}$, the number of iterations needed to meet a tolerance that scales with the order of the method is small.

5 Numerical experiments

We present numerical examples in Section 5.1 to verify convergence property of the proposed method. In all experiments, the classical Runge-Kutta method is used for time integration. The L_2 errors at final time are computed as

$$\|\mathbf{u}_h - \mathbf{u}_{ex}\| = \sqrt{h^d(\mathbf{u}_h - \mathbf{u}_{ex})^T(\mathbf{u}_h - \mathbf{u}_{ex})},$$

where \mathbf{u}_h is the numerical solution, \mathbf{u}_{ex} is the manufactured solution restricted to the grid, h is the grid spacing and d is the spatial dimension. The convergence rates for grids refined by a factor of two are estimated by

$$\log_2 \frac{\|\mathbf{u}_{2h} - \mathbf{u}_{ex}\|}{\|\mathbf{u}_h - \mathbf{u}_{ex}\|}.$$

In Section 5.2, we test the preconditioned conjugate gradient method for solving 2D wave equation with variable coefficient.

5.1 Examples in one space dimension

We start with a verification of convergence rate for the wave equation (3) with a constant wave speed $c = 1$ in the domain $x \in [-\pi/2, \pi/2]$ and $t \in [0, 2]$. We consider the Dirichlet boundary conditions at $x = -\pi/2$ and $x = \pi/2$. The boundary data is obtained from the manufactured solution $U = \cos(10x + 1) \cos(10t + 2)$.

In the semi-discretization (9)-(10), we use the SBP operators constructed in [18] of fourth and sixth order of accuracy. We are interested in how the dissipative term affects the accuracy of the numerical solution. To this end, we consider the parameter $\beta = 0$ or -1 to control the dissipation. The L_2 errors and the corresponding rates of convergence are presented in Table 1 for the fourth order method and Table 2 for the sixth order method.

$\beta = 0$			$\beta = -1$		
n	L_2 error	rate	n	L_2 error	rate
101	1.1469×10^{-2}		101	5.8872×10^{-4}	
201	1.5189×10^{-3}	2.9166	201	3.5251×10^{-5}	4.0618
401	1.9285×10^{-4}	2.9775	401	2.1593×10^{-6}	4.0290
801	2.4215×10^{-5}	2.9934	801	1.3419×10^{-7}	4.0082
1601	3.0314×10^{-6}	2.9978	1601	8.3723×10^{-9}	4.0025

Table 1: The fourth order SBP-SAT method for the one dimensional wave equation in a single domain.

We observe that the parameter β affects the numerical errors and convergence rates. For the fourth order method, fourth order convergence rate is obtained when $\beta = -1$. However, when

$\beta = 0$		
n	L_2 error	rate
101	3.4741×10^{-3}	
201	1.1656×10^{-4}	4.8975
401	3.7103×10^{-6}	4.9733
801	1.1652×10^{-7}	4.9929
1601	3.6466×10^{-9}	4.9979

$\beta = -1$		
n	L_2 error	rate
101	7.4933×10^{-5}	
201	1.4300×10^{-6}	5.7155
401	2.9257×10^{-8}	5.6111
801	6.1548×10^{-10}	5.5709
1601	1.3250×10^{-11}	5.5377

Table 2: The sixth order SBP-SAT method for the one dimensional wave equation in a single domain.

$\gamma = 0$		
n	L_2 error	rate
51	1.6233×10^{-4}	
101	6.9416×10^{-6}	4.5475
201	3.3128×10^{-7}	4.3892
401	1.8150×10^{-8}	4.1900
801	1.0787×10^{-9}	4.0726

$\gamma = -1$		
n	L_2 error	rate
51	1.2908×10^{-4}	
101	6.6070×10^{-5}	4.2881
201	3.2790×10^{-6}	4.3327
401	1.8134×10^{-7}	4.1764
801	1.0788×10^{-9}	4.0715

Table 3: The fourth order SBP-SAT method for the one dimensional wave equation with a grid interface.

$\beta = 0$ the convergence rate drops by one order to three. This agrees with the error estimate in Section 3.2. For the sixth order method, the choice $\beta = -1$ leads to a super-convergence of order 5.5, which is also observed in [25]. Without dissipation from the Dirichlet boundary, however, the convergence rate is five.

To further test the numerical interface treatment (27)-(30), we consider the same problem as above but with a grid interface at $x = 0$ and interface conditions (25)-(26). To eliminate any influence from the boundaries, we impose periodic boundary condition at $x = \pm\pi/2$. For the interface conditions, we choose either $\gamma = -1$ or $\gamma = 0$, corresponding to with or without dissipation at the interface, respectively. The L_2 errors and the corresponding rates of convergence are presented in Table 3 for the fourth order method and Table 4 for the sixth order method.

For the fourth order method, both $\gamma = 0$ and $\gamma = -1$ lead to a convergence rate of order four. For the same mesh resolution, the L_2 errors are almost the same. For the sixth order method, the two choices of γ give different rates of convergence. The convergence rate with $\gamma = -1$ is 5.5, but the rate drops to between 5 and 5.5 when $\gamma = 0$. On the finest mesh, the L_2 error with the dissipative discretization is about half of the L_2 error with the energy-conserving discretization.

$\gamma = 0$		
n	L_2 error	rate
51	9.4638×10^{-5}	
101	1.4000×10^{-6}	6.0790
201	3.1396×10^{-8}	5.4786
401	8.1443×10^{-10}	5.2686
801	2.2536×10^{-11}	5.1755

$\gamma = -1$		
n	L_2 error	rate
51	5.0107×10^{-5}	
101	1.2083×10^{-6}	5.3739
201	2.6278×10^{-8}	5.5230
401	5.7619×10^{-10}	5.5112
801	1.2723×10^{-11}	5.5010

Table 4: The sixth order SBP-SAT method for the one dimensional wave equation with a grid interface.

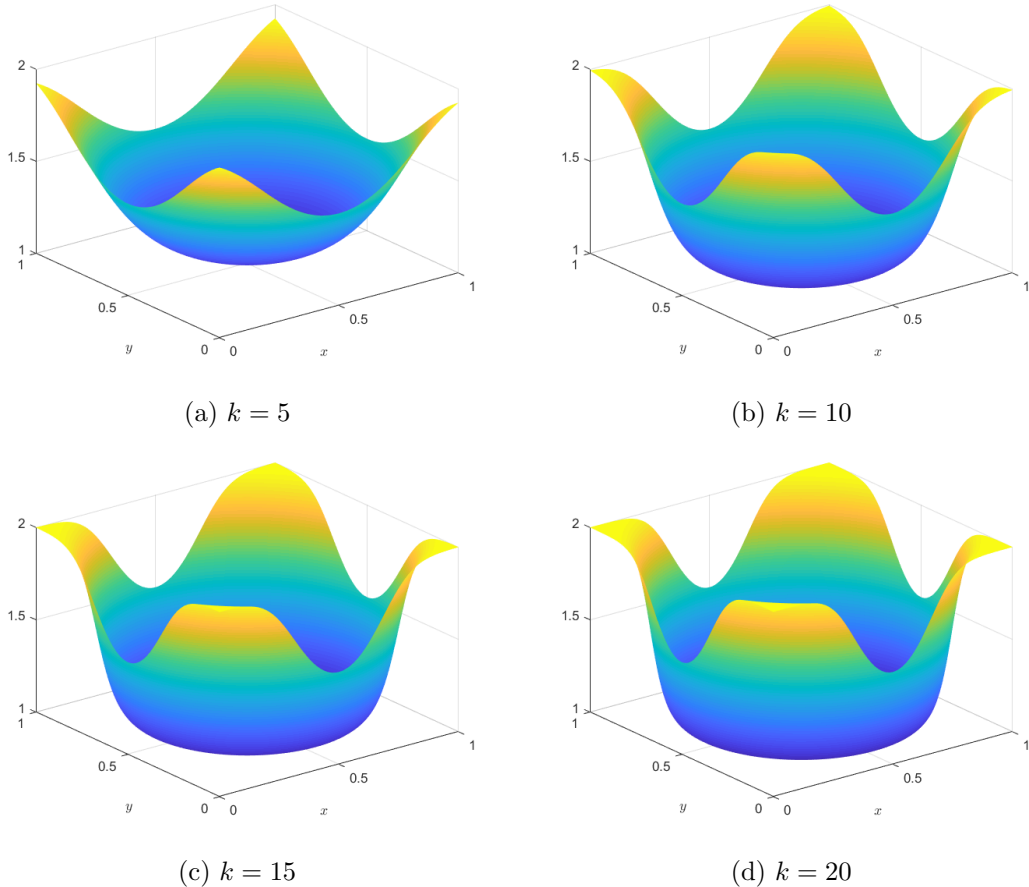


Figure 1: Material property

5.2 Examples in two space dimensions

We consider variable coefficient problem (31) with $a(x, y) = 0.5(\tanh(k(R - 0.25)) + 3)$ and $b(x, y) = 0.5(\tanh(k(R - 0.25)) + 3)$, where $R = (x - 0.5)^2 + (y - 0.5)^2$. The parameters a and b model heterogeneous material properties of a layered structure, with k controlling the transition of two layers. A few examples of $a(x, y)$ with different values of k are shown in Figure 1. We see that with a larger k , the transition zone of two materials becomes smaller. We choose the forcing function F so that the manufactured solution $U = \cos(2x + \pi/2) \cos(2y + \pi/2) \cos(2\sqrt{2}t + 3)$ satisfies the equations.

The equations are discretized in space by the scheme (32)-(33) with the second derivative variable coefficients SBP operators constructed in [15]. The classical Runge-Kutta method is used to advance the semi-discretization in time. At each Runge-Kutta stage, the linear system is solved by a preconditioned conjugate gradient (PCG) method, where the preconditioner is obtained by the incomplete Cholesky (ICHOL) factorization. Since the matrix \mathbf{A} is only semi-definite, in the ICHOL process we increase the diagonal elements by 1% and 0.01% for the fourth and sixth order methods, respectively. In addition, to keep the factorized matrix sparse, we use a drop-tolerance 10^{-4} and 10^{-6} for the fourth and sixth order methods, respectively. In Table 5, the number of iterations (averaged in the four Runge-Kutta stages at all time steps) are shown for different material properties and mesh resolutions. We observe that in all cases we have tested, PCG converges with less than four iterations.

Fourth order					Sixth order				
n	$k = 5$	$k = 10$	$k = 15$	$k = 20$	n	$k = 5$	$k = 10$	$k = 15$	$k = 20$
16^2	2.6	1.9	1.3	1.1	16^2	1.0	1.0	1.0	1.0
31^2	3.1	2.3	1.6	1.3	31^2	1.1	1.2	1.3	1.4
61^2	3.3	2.6	1.8	1.4	61^2	1.4	1.5	1.8	1.9
121^2	3.5	2.7	2.0	1.5	121^2	2.2	2.2	2.5	2.8

Table 5: Number of iterations for solving the linear system: the fourth (left) and sixth (right) order SBP-SAT method for the two dimensional wave equation.

6 Conclusion

We have developed an energy-based SBP-SAT discretization of the wave equation. Comparing with the traditional SBP-SAT discretization, an advantage of the proposed method is that no mesh-dependent parameter is needed to imposed Dirichlet boundary conditions and material interface conditions. Our stability analysis shows that the discretization can either be energy conserving or dissipative. In addition, we have presented a general framework for deriving error estimates by the normal mode analysis and detailed the accuracy analysis for a fourth order discretization.

In numerical experiments, we have examined more cases for the effect of dissipation on the convergence rate. For the fourth order method, dissipation at a Dirichlet boundary increases convergence rate from 3 to 4, which is also theoretically proved; while at a grid interface, both dissipative and energy-conserving interface coupling lead to a fourth order convergence rate. For the sixth order method, dissipation at a Dirichlet boundary increases convergence rate from 5 to 5.5. At a grid interface, similar improvement is also observed.

For the energy-based discretization to be efficient the vector \mathbf{u}_t must be isolated and we have demonstrated that this is possible. For problems in one space dimension this can be done by explicitly or implicitly forming the pseudo inverse and extracting a few of its columns. For problems in multiple dimensions with constant coefficients, we have leveraged the diagonalization technique from [28]. This technique gives an algorithm with the same cost as a traditional method of lines discretization after a pre-computation step that only involve solving one dimensional eigenvalue problems. The same procedure cannot be generalized to problems with variable coefficients. However, our numerical experiments have demonstrated that the corresponding linear system can be solved efficiently by the conjugate gradient method with an incomplete Cholesky preconditioner. The iterative solver converges fast and is insensitive to material property and mesh resolution.

References

- [1] M. Almquist and E. M. Dunham. Non-stiff boundary and interface penalties for narrow-stencil finite difference approximations of the laplacian on curvilinear multiblock grids. *J. Comput. Phys.*, 408:109294, 2020.
- [2] M. Almquist, S. Wang, and J. Werpers. Order-preserving interpolation for summation-by-parts operators at nonconforming grid interfaces. *SIAM J. Sci. Comput.*, 41:A1201–A1227, 2019.
- [3] D. Appelö and T. Hagstrom. A new discontinuous Galerkin formulation for wave equations in second-order form. *SIAM J. Numer. Anal.*, 53:2705–2726, 2015.

- [4] D. Appelö and T. Hagstrom. An energy-based discontinuous Galerkin discretization of the elastic wave equation in second order form. *Comput. Methods Appl. Mech. Engrg.*, 338:362–391, 2018.
- [5] D. Appelö and G. Kreiss. Application of a perfectly matched layer to the nonlinear wave equation. *Wave Motion*, 44:531–548, 2007.
- [6] D. Appelö and S. Wang. An energy based discontinuous Galerkin method for coupled elasto-acoustic wave equations in second order form. *Int. J. Numer. Meth. Eng.*, 119:618–638, 2019.
- [7] M. H. Carpenter, D. Gottlieb, and S. Abarbanel. Time-stable boundary conditions for finite-difference schemes solving hyperbolic systems: methodology and application to high-order compact schemes. *J. Comput. Phys.*, 111:220–236, 1994.
- [8] K. Duru and K. Virta. Stable and high order accurate difference methods for the elastic wave equation in discontinuous media. *J. Comput. Phys.*, 279:37–62, 2014.
- [9] S. Eriksson and S. Wang. Summation-by-parts approximations of the second derivative: Pseudoinverses of singular operators and revisiting the sixth order accurate narrow-stencil operator. *arXiv: 2011.03776*, 2020.
- [10] M. J. Grote, A. Schneebeli, and D. Schötzau. Discontinuous Galerkin finite element method for the wave equation. *SIAM. J. Numer. Anal.*, 44:2408–2431, 2006.
- [11] B. Gustafsson, H. O. Kreiss, and J. Olinger. *Time-Dependent Problems and Difference Methods*. John Wiley & Sons, 2013.
- [12] W. D. Henshaw. A high-order accurate parallel solver for Maxwell’s equations on overlapping grids. *SIAM J. Sci. Comput.*, 28:1730–1765, 2006.
- [13] J. E. Hicken and D. W. Zingg. Summation-by-parts operators and high-order quadrature. *J. Comput. Appl. Math.*, 237:111–125, 2013.
- [14] H. O. Kreiss and J. Olinger. Comparison of accurate methods for the integration of hyperbolic equations. *Tellus*, 24:199–215, 1972.
- [15] K. Mattsson. Summation by parts operators for finite difference approximations of second-derivatives with variable coefficient. *J. Sci. Comput.*, 51:650–682, 2012.
- [16] K. Mattsson, F. Ham, and G. Iaccarino. Stable and accurate wave-propagation in discontinuous media. *J. Comput. Phys.*, 227:8753–8767, 2008.
- [17] K. Mattsson, F. Ham, and G. Iaccarino. Stable boundary treatment for the wave equation on second-order form. *J. Sci. Comput.*, 41:366–383, 2009.
- [18] K. Mattsson and J. Nordström. Summation by parts operators for finite difference approximations of second derivatives. *J. Comput. Phys.*, 199:503–540, 2004.
- [19] A. Nissen, G. Kreiss, and M. Gerritsen. Stability at nonconforming grid interfaces for a high order discretization of the Schrödinger equation. *J. Sci. Comput.*, 53:528–551, 2012.
- [20] N. A. Petersson and B. Sjögreen. Stable grid refinement and singular source discretization for seismic wave simulations. *Commun. Comput. Phys.*, 8:1074–1110, 2010.
- [21] B. Sjögreen and N. A. Petersson. A fourth order accurate finite difference scheme for the elastic wave equation in second order formulation. *J. Sci. Comput.*, 52:17–48, 2012.

- [22] M. Svärd and J. Nordström. On the convergence rates of energy-stable finite-difference schemes. *J. Comput. Phys.*, 397:108819, 2019.
- [23] K. Virta and K. Mattsson. Acoustic wave propagation in complicated geometries and heterogeneous media. *J. Sci. Comput.*, 61:90–118, 2014.
- [24] S. Wang. An improved high order finite difference method for non-conforming grid interfaces for the wave equation. *J. Sci. Comput.*, 77:775–792, 2018.
- [25] S. Wang and G. Kreiss. Convergence of summation-by-parts finite difference methods for the wave equation. *J. Sci. Comput.*, 71:219–245, 2017.
- [26] S. Wang, A. Nissen, and G. Kreiss. Convergence of finite difference methods for the wave equation in two space dimensions. *Math. Comp.*, 87:2737–2763, 2018.
- [27] S. Wang, K. Virta, and G. Kreiss. High order finite difference methods for the wave equation with non-conforming grid interfaces. *J. Sci. Comput.*, 68:1002–1028, 2016.
- [28] L. Zhang, D. Appelö, and T. Hagstrom. Energy-based discontinuous Galerkin difference methods for second-order wave equations. *Commun. Appl. Math. Comput. (submitted)*, 2020.